[redacted]

GPO PRICE $ _____

CFSTI PRICE(S) $ _____

Hard copy (HC) 2.00

Microfiche (MF) .50

ff 653 July 65

[redacted]

GENERAL DYNAMICS

Convair Division

[redacted]

A2136-1 (REV. 5-65)

N67 14557

(ACCESSION NUMBER)	(THRU)
42	1
(PAGES)	(CODE)
CR-80892	31
(NASA CR OR TMX OR AD NUMBER)	(CATEGORY)

FACILITY FORM 602

RANGE SAFETY AERODYNAMICS DATA FOR ATLAS/CENTAUR/SURVEYOR DIRECT ASCENT FLIGHTS

GDC-BTD66-034

4 May 1966

Contract NAS3-8701

Prepared by T. Chacon
T. Chacon

Checked by D. H. Lesney
D. H. Lesney

Approved by F. B. Anthony
F. B. Anthony
Research Group Engineer

Approved by R. S. Wentink
R. S. Wentink
Assistant Chief Engineer
Design Analysis -
Launch Vehicle Project

GENERAL DYNAMICS
Convair Division

FOREWORD

This report presents a summary of the aerodynamic data required by the Range Safety Division, ETR, for the establishment of range safety criteria for Atlas/Centaur/Surveyor direct ascent flights.

This report fulfills a contractual requirement (Item 88 of Centaur Documentation Requirements Plan, Report No. 55-00207F, 18 March 1966) which specifies that the Convair Division of General Dynamics shall provide vehicle aerodynamic, weight, and destruct action data required for ETR support planning and range safety.

SUMMARY

Atlas/Centaur/Surveyor range safety aerodynamics data are presented for use by the Range Safety Division of the AFMTC at Cape Kennedy, Florida.

Nominal impact points and impact dispersion envelopes are given for the Atlas booster and sustainer stage and for the Centaur insulation panels and nose fairing. Impact information covers the full range of trajectories targeted for the AC-10 launch opportunities (launch azimuths from 84 deg to 115 deg and injection flight path angles from approximately -5 deg to +7 deg). Supplemental data are presented to extend the range of launch azimuths to 80 deg.

To support a detailed analysis of the effects of destruct action or premature flight termination, applicable drag coefficients and vehicle fragmentation data are presented. In accordance with range safety requirements, results of an investigation of the possible number of resulting fragments and a drag and velocity analysis for fifteen of the major fragments are given. Power-off drag coefficients for various stage combinations are presented to support an analysis of the effects of premature flight termination.

The impact data presented in this report were derived from trajectories targeted for the AC-10 vehicle, but the results are applicable for all direct ascent missions of Atlas/Centaur/Surveyor. Addenda will be published to incorporate changes pertinent to specific flight vehicles.

TABLE OF CONTENTS

LIST OF ILLUSTRATIONS

LIST OF TABLES

INTRODUCTION

Range safety aerodynamics data for Atlas/Centaur flights are prepared in compliance with AFMTC range safety requirements (Reference 1) which specify that ETR users must supply the following:

a. The expected impact point for each stage and jettisoned body in terms of geodetic latitude and longitude in decimal degrees, and range from pad to impact in nautical miles.

b. Estimates of the range and cross-range rms dispersions (or standard deviations) for each stage or re-entry body, assuming a normally functioning vehicle.

c. Expected effects of destruct explosion including the number and approximate weights of resulting fragments, estimates of drag coefficient histories for 10 to 15 major fragments, effect of explosion on remaining fuel and stage, and effects of explosion in the form of velocity increments for the major fragments.

SECTION 1

TRAJECTORY CHARACTERISTICS

A detailed description of direct ascent trajectories is presented in Reference 2; however, as an aid to the reader, a brief description of this mode of orbital injection is included below.

The direct ascent mode is characterized by a continuous powered-flight phase from launch to orbital injection. To accomodate varying launch site-target geometry during the daily launch window (the launch site moves in an easterly direction) the launch azimuth (Σ) is advanced in a southerly direction. In order to satisfy the angular relationship, the injection flight path angle (γ)† is varied. Since the relationship between Σ and γ is unique for any given launch time, there results a large number of possible trajectories for any given launch opportunity.

Varying injection flight path angle has a pronounced effect on the powered-phase flight profile. The booster phase of the flight profile remains unchanged, but the remaining trajectory is a strong function of injection γ.

† Flight path angle is defined as the angle between the inertial velocity vector and the local horizontal plane; i.e., the plane normal to the geocentric position vector. It is measured positive above the plane.

SECTION 2

ANALYSIS OF IMPACT LOCATIONS FOR JETTISONED ITEMS

Consistent with the requirements of Reference 1, nominal and three-sigma impact locations have been generated for items jettisoned during normal flight. Following the nominal Atlas/Centaur/Surveyor flight plan these items are: (1) Atlas booster package. (2) Centaur insulation panels, (3) Centaur nose fairing, and (4) Atlas sustainer stage. In addition to three-sigma flight considerations, dispersion envelopes reflect the effects of possible breakup of re-entering hardware.

Because of the uncertainties involved in estimating drag histories for the jettisoned items and because downrange wind conditions are relatively uncertain, efforts have been directed toward making impact dispersion envelopes conservative. In addition to the use of extreme wind profiles, wind and drag data have been combined in the manner which produces the greatest possible dispersion.

Effects of an oblate, rotating earth were accounted for in all freefall simulations, and a zero lift condition was assumed for all re-entry hardware.

2.1 NOMINAL IMPACT POINTS. Nominal impact data were generated by means of Reference 3 computer program utilizing initial position and velocity data that were obtained from the listings in Reference 4. The program was used to simulate hardware freefall re-entry assuming a combination of model atmospheres (References 14 and 15) and nominal June winds.

Since all re-entering hardware is considered to be aerodynamically unstable, nominal drag effects were accounted for by using "tumbling" drag data. (Tumbling drag is defined as an average of drag experienced at 0-, 90-, 180-, and 270-degree angles of attack. Derivation of the relation is presented in Appendix A.) Drag histories, obtained from data in References 6 and 7 and by theoretical methods, are presented in Figures 2-1 through 2-5.

Re-entry simulation of Atlas sustainer stage included the effects of retrorocket firing. This was accomplished by simulating a reverse thrust of 5600 lb for 0.7 second following sustainer separation.

Inspection of resulting atmosphere re-entry data (and of vacuum re-entry data) indicated that impact downrange distance varied linearly with flight path angle between $\gamma = -5.4$ deg and +3 deg and also between $\gamma = +3$ deg and +6.7 deg.

2.2 IMPACT DISPERSION ENVELOPES. Impact dispersion envelopes were obtained by means of Reference 5 computer program. Initiation of freefall for each of the four major jettisoned items was accomplished by utilizing nominal position and three-sigma velocity

data (Reference 4). The latter data were generated to simulate three-sigma maximum, minimum, nose-right, and nose-left vehicle performance. Drag and wind combinations used to generate dispersion impact points are given in Table 2-1. Maximum and minimum drag are designated by $\alpha = 90$ and 0 deg, respectively, in the drag coefficient curves of Figures 2-1 through 2-5. Both maximum and minimum drag were used in the lateral performance cases to ensure attainment of the greatest possible lateral dispersions.

To compensate for the uncertainty of downrange conditions, three-sigma NASA mean annual winds (Reference 8) were used for the impact dispersion analysis. The dispersions produced by these extreme wind conditions are considered conservative.

Since re-entering hardware may break up due to aerodynamic loading or heating, impact points were generated for maximum, minimum, and lateral 3σ dispersions of possible resulting fragments. To accomplish this, each of the four major jettisoned items was assumed to disintegrate at approximately one-g deceleration. Consistent with Reference 13, limiting values of $C_DA/W = 1.0$ and 0.001 were assumed for the minimum- and maximum-distance fragments, respectively. The maximum nose-left and nose-right re-entry fragments utilized both maximum (1.0) and minimum (0.001) values of C_DA/W.

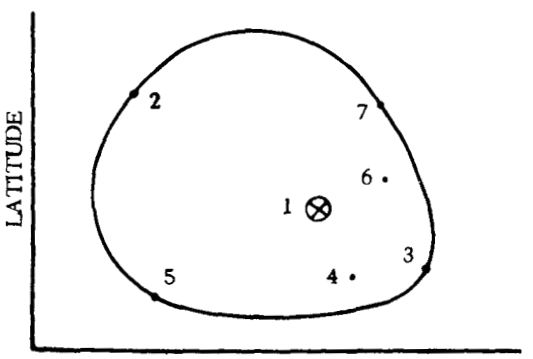

Example of Fragment Impact Dispersion Envelope

Table 2-1. Drag Coefficients and Winds Used for Impact Dispersions

CASE	DRAG	WIND DIRECTION*
Nominal	Tumbling	Mean Annual
Maximum Dispersion	Minimum	North and West
Minimum Dispersion	Maximum	South and East
Right Dispersion	Maximum and Minimum	North and East
Left Dispersion	Maximum and Minimum	South and West

*From the indicated direction.

Wind and drag combinations used for the fragment re-entry cases are indicated in Table 2-1. Previous analyses have shown that dispersion envelopes are established by assumed fragments from the major jettisoned items rather than by the major items themselves, so that only the fragment dispersion impact points were calculated.

Dispersion envelopes were obtained graphically as illustrated (page 2-2) to include all calculated fragment impact points. Impact dispersion criteria associated with the illustration are listed in Table 2-2.

Reference 5 computer program was designed to accomplish essentially the same type of atmosphere re-entry simulation as Reference 3. The former program was chosen for the dispersion impact analysis in order to avoid problems in numerical instability associated with re-entry simulation of fragments with a ballistic parameter $C_D A/W$ equal to 1.0. Fragments in this category tend to float during re-entry into the atmosphere, and their direction of motion is severely influenced by winds. In order to be able to follow this type of motion, a program must have the capability of significantly varying the numerical integration time step.

2.3 RESULTS. Nominal impact points and impact dispersion envelopes are presented in Figure 2-6. Presentation of geodetic latitude and longitude in a Cartesian coordinate system is considered sufficiently accurate for the purpose intended. The earth traces presented for launch azimuths of 80 deg to 115 deg are actually vacuum instantaneous impact point (IIP) traces which were obtained from nominal trajectory listings (Reference 4) for these launch azimuths. (The IIP traces are presented rather than the sub-vehicle traces in an effort to include the effects of earth rotation during the time interval from staging to impact.) Even though the vacuum and aerodynamic times to impact do not correspond, the errors that are introduced are negligible. Inspection of the IIP earth traces shows evidence of guidance yaw steering at the higher launch azimuths. The traces appear to deviate in a northerly direction.

In an effort to simplify the presentation of impact data, nominal impact points are plotted in Figure 2-6 for an injection flight path angle (γ) equal to +6.70 and a launch azimuth (Σ) of 114 degrees. The loci of nominal impact points at other pertinent launch azimuths are indicated on the same figure for different values of γ. A linear variation of γ exists along any Σ in the interval $-5.4 \text{ deg} \leq \gamma \leq +3 \text{ deg}$. Between $\gamma = +3$ deg and +6.70 deg the impact points do not vary.

Impact dispersion envelopes are also shown in Figure 2-6. Although individual dispersions are slightly dependent on Σ and γ, it is recommended that the given envelopes be used for all values of Σ and γ. (This is permissile since investigation shows that dispersions are somewhat smaller at the more negative values of γ and since conservative assumptions of drag coefficient and winds were used in determining the impact envelopes.) The method of transposing the location of the impact dispersion envelopes to correspond to any possible set of Σ - γ values is explained and illustrated in Figure 2-6. To facilitate transposition of the envelopes, a set of templates is provided.

Table 2-2. Impact Dispersion Criteria

IMPACT† POINT	POWERED TRAJECTORY	FRAGMENTATION ASSUMED	C_DA/W	WINDS*
1	Nominal	No	Nominal	Nominal
2	Min. Perform	Yes	1.0	3σ
3	Max. Perform	Yes	0.001	3σ
4	Max. Right	Yes	0.001	3σ
5	Max. Right	Yes	1.0	3σ
6	Max. Left	Yes	0.001	3σ
7	Max. Left	Yes	1.0	3σ

* 3σ N-S and E-W wind components were combined in the manner which produced the greatest dispersion.

† Numbers correspond to example on Page 2-2.

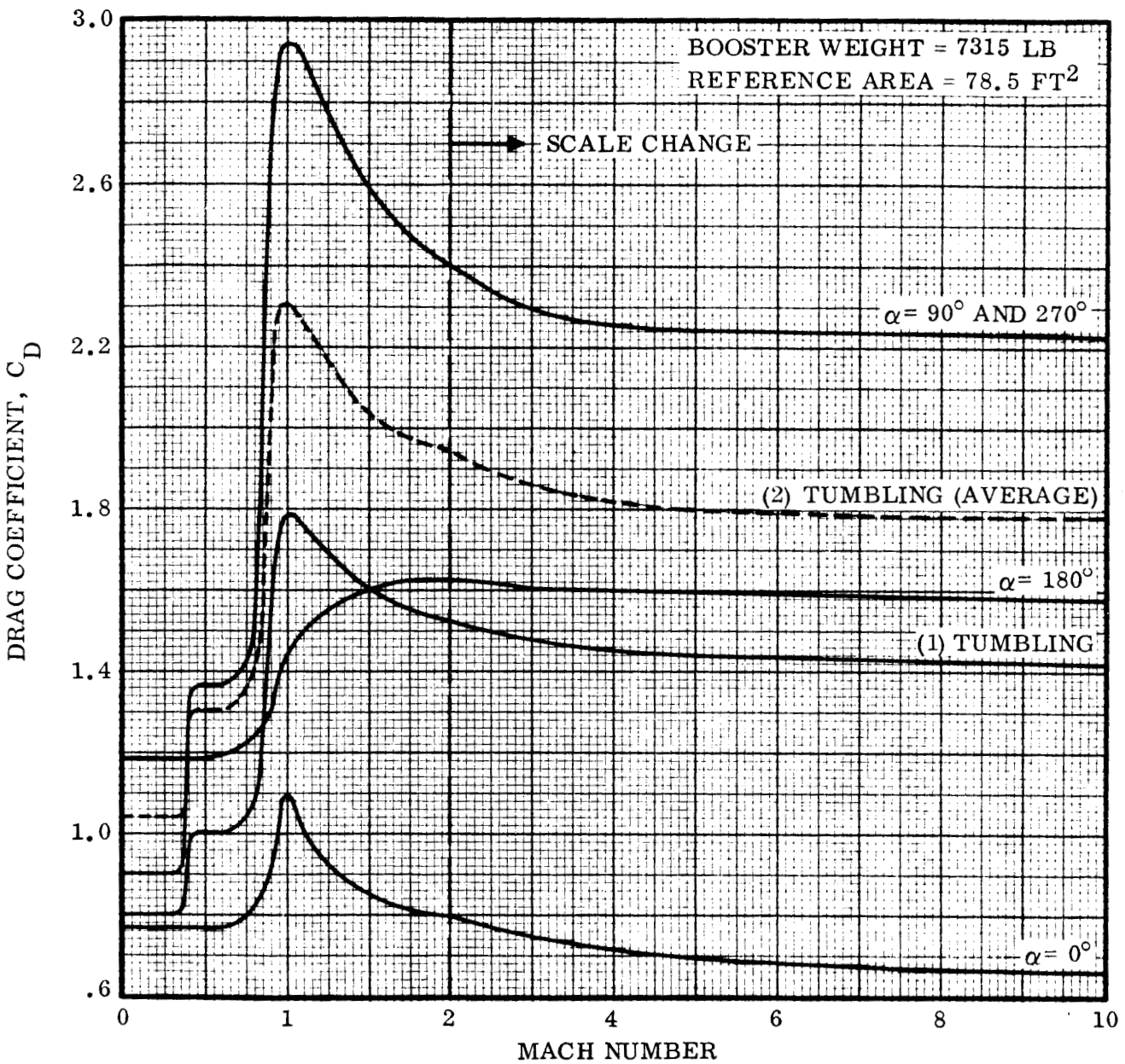

(1) About pitch axis
(2) Average for tumbling about pitch and yaw axes

Figure 2-1. Drag Coefficients for Atlas Booster Package (Minimum C_D Estimate)

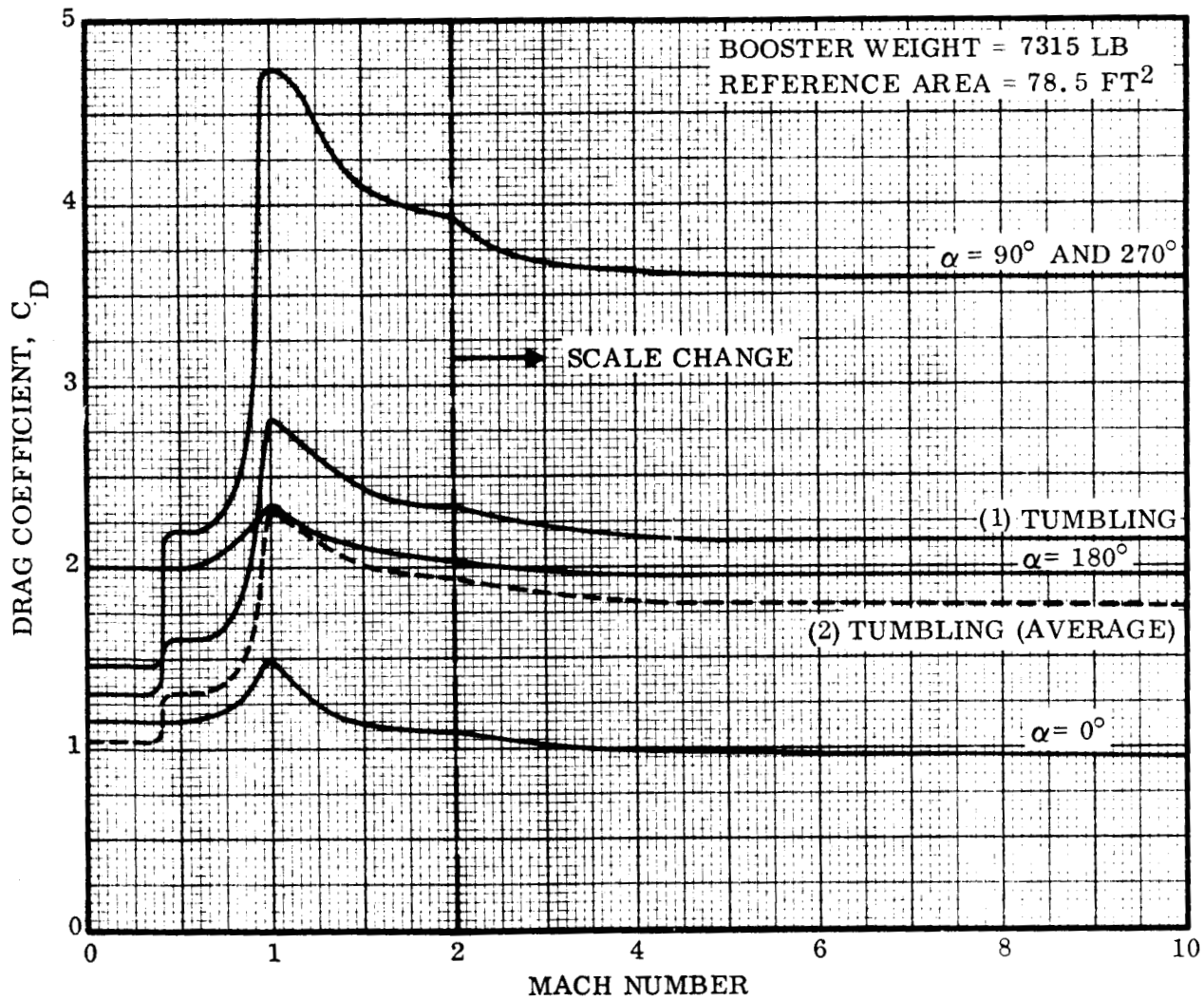

(1) About yaw axis
(2) Average for tumbling about pitch and yaw axes

Figure 2-2. Drag Coefficients for Atlas Booster Package (Maximum C_D Estimate)

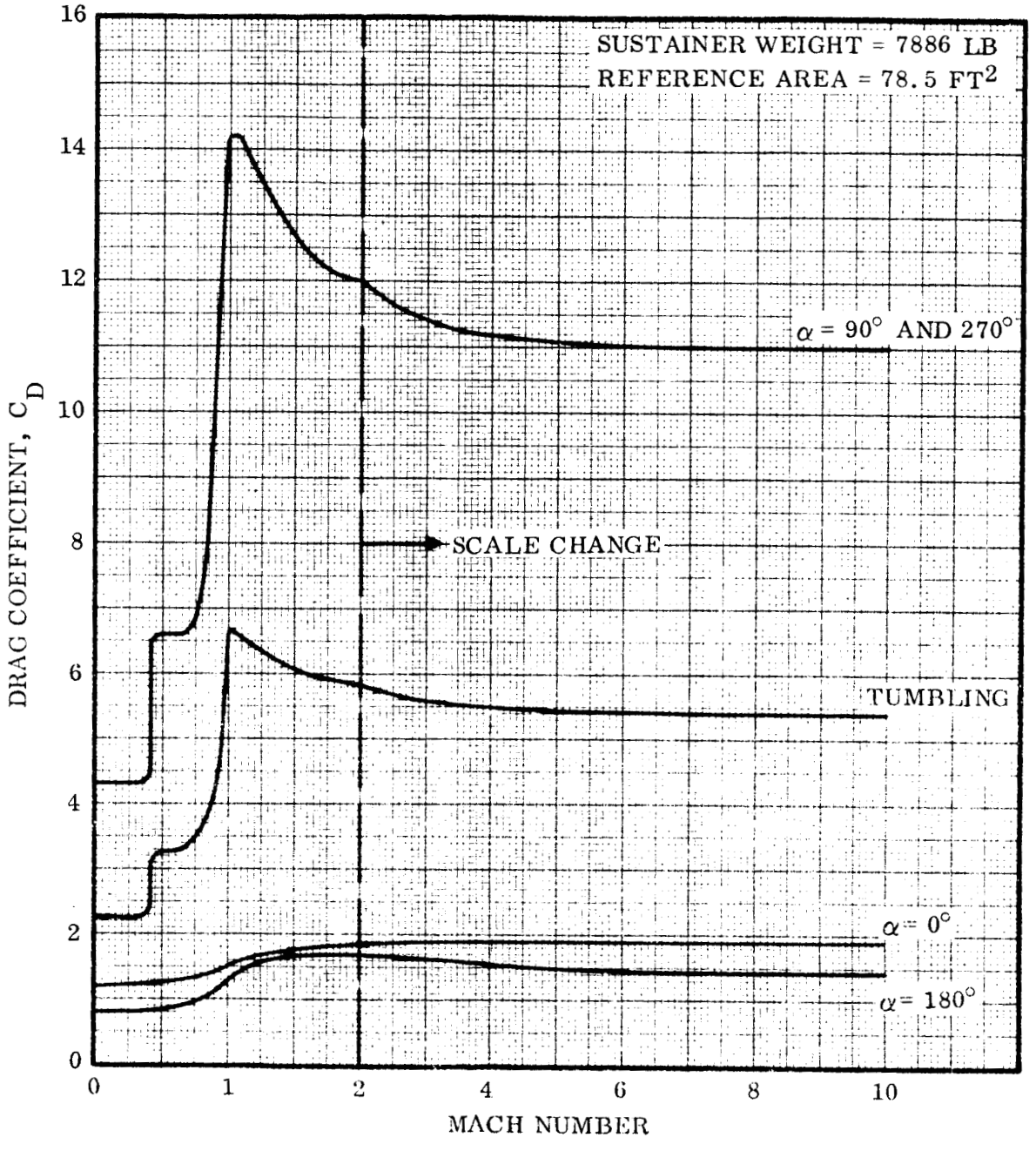

Figure 2-3. Drag Coefficients for Atlas Sustainer Stage

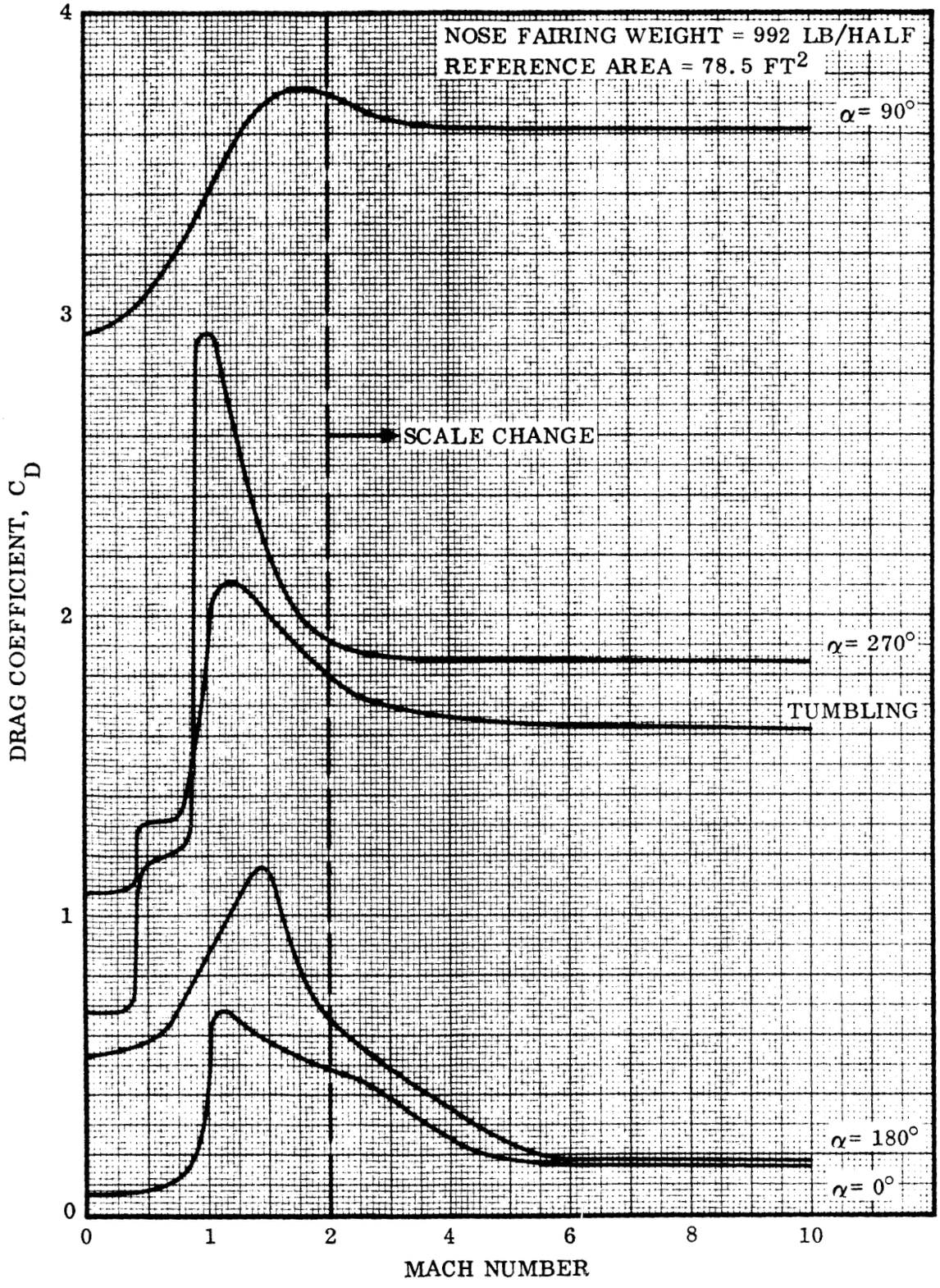

Figure 2-4. Drag Coefficients for Centaur Nose Fairing

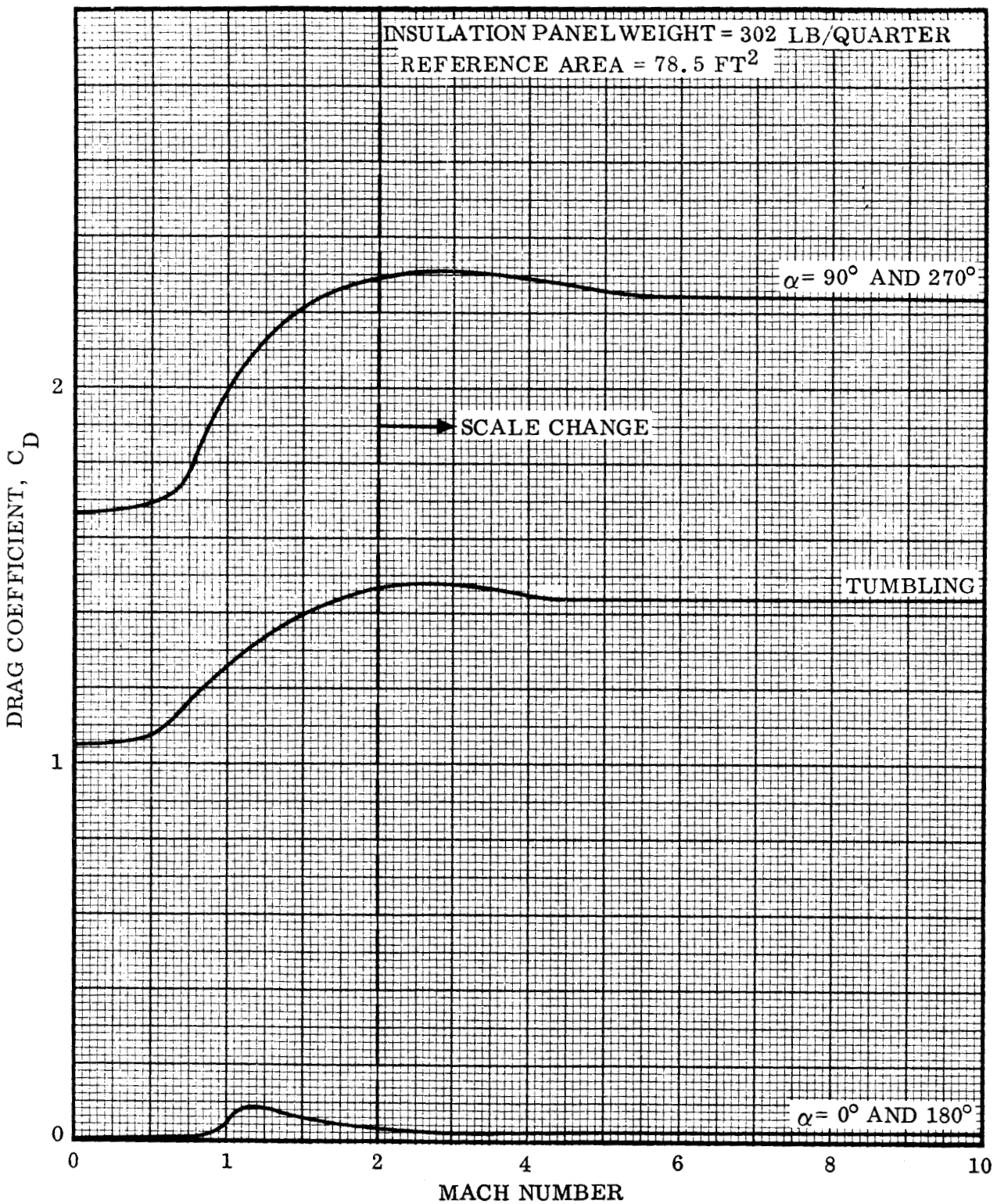

Figure 2-5. Drag Coefficients for Centaur Insulation Panels

NOTES:

1. NOM. I.P. = NOMINAL IMPACT POINT(S).

   Σ = LAUNCH AZIMUTH

   γ = FLIGHT PATH ANGLE OF VEHICLE AT TIME OF INJECTION INTO MISSION ORBIT (MECO).

2. NOMINAL IMPACT POINTS ARE FUNCTIONS OF Σ AND γ EXCEPT FOR ATLAS BOOSTER PACKAGE, WHICH VARIES WITH Σ ONLY. (NOMINAL TRAJECTORY PROFILE TO THE TIME OF BOOSTER JETTISON IS INVARIANT WITH γ.)

3. TYPICAL IMPACT DISPERSION ENVELOPES (SOLID OVALS) ARE SHOWN FOR $\Sigma = 114^{\circ}$ AND $\gamma = +6.70^{\circ}$. NOMINAL IMPACT POINTS ASSOCIATED WITH THESE ENVELOPES ARE CIRCLED THUS ⊕ ENVELOPES INCLUDE EFFECTS OF 1) ALL GUIDANCE AND PERFORMANCE DISPERSIONS, 2) ASSUMED FRAGMENTATION OF STRUCTURE DURING RE-ENTRY, 3) 3-SIGMA E-W AND N-S WIND COMPONENTS COMBINED IN THE MOST ADVERSE MANNER, AND 4) EXTREMES OF RE-ENTRY DRAG COEFFICIENTS.

4. DISPERSION ENVELOPES FOR ALL VALUES OF Σ AND γ ARE CONGRUENT TO THOSE SHOWN. TO LOCATE ENVELOPES FOR OTHER VALUES OF Σ AND γ, ROTATE AND/OR TRANSLATE THE ENVELOPES TO THE APPLICABLE VALUES OF Σ AND γ. THE DASHED OVAL IS AN ILLUSTRATION OF THIS TECHNIQUE, SHOWING THE DISPERSION ENVELOPE OF THE ATLAS SUSTAINER FOR $\Sigma = 99^{\circ}$. $\gamma = -5.4^{\circ}$.

5. ADDITIONAL DISPERSION ENVELOPES ARE DRAWN TO SCALE ON THE RIGHT OF THE ILLUSTRATION; THESE FIGURES MAY BE CUT OUT AND USED AS TEMPLATES IF DESIRED.

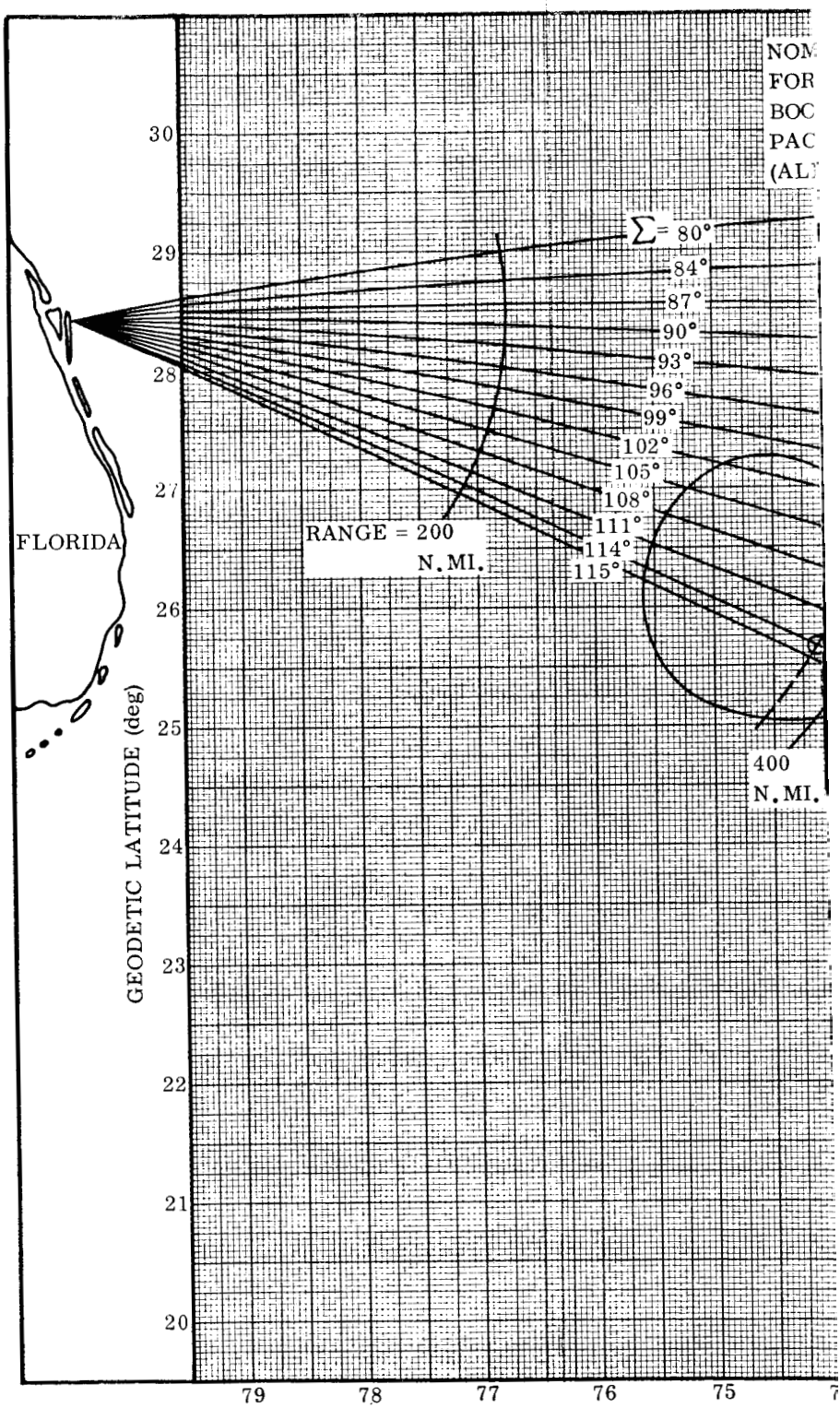

Figure 2-6. Loci of Nominal Impact Points and Typical Impact Dispersion Envelopes for Items Jettisoned During Normal Flight

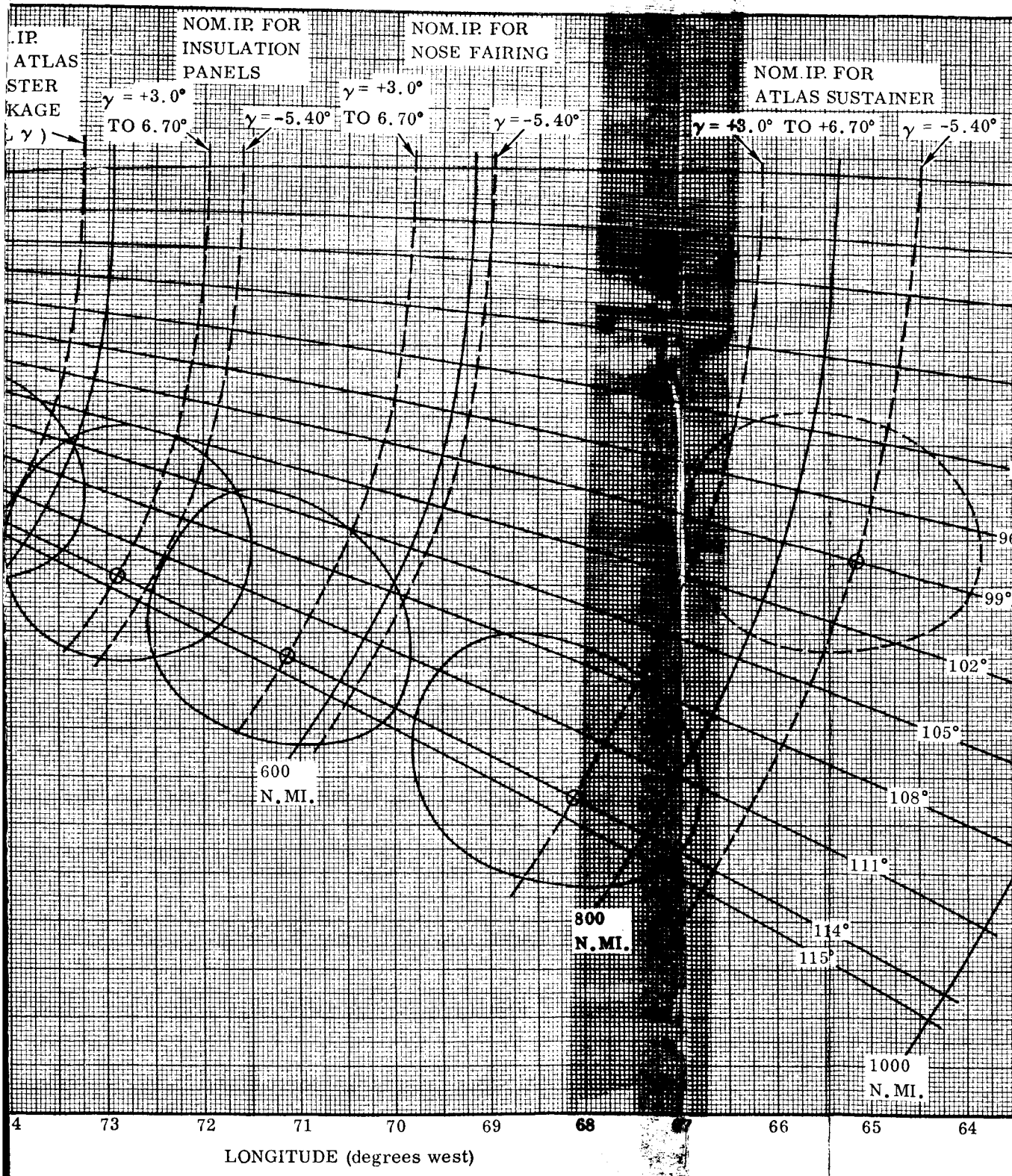
.IP.
ATLAS
STER
KAGE
, γ)
NOM.IP. FOR
INSULATION
PANELS
γ = +3.0°
TO 6.70°
γ = -5.40°
NOM.IP. FOR
NOSE FAIRING
γ = +3.0°
TO 6.70°
γ = -5.40°
NOM.IP. FOR
ATLAS SUSTAINER
γ = +3.0° TO +6.70°
γ = -5.40°
600
N.MI.
800
N.MI.
1000
N.MI.
96°
99°
102°
105°
108°
111°
114°
115°
4
73
72
71
70
69
68
67
66
65
64
LONGITUDE (degrees west)

2-10-2

NOTE: CUT OUT TEMPLATES. PUNCH HOLES AT NOMINAL IMPACT POINTS ON TEMPLATES TO AID IN LOCATING DISPERSION ENVELOPES ON MAP

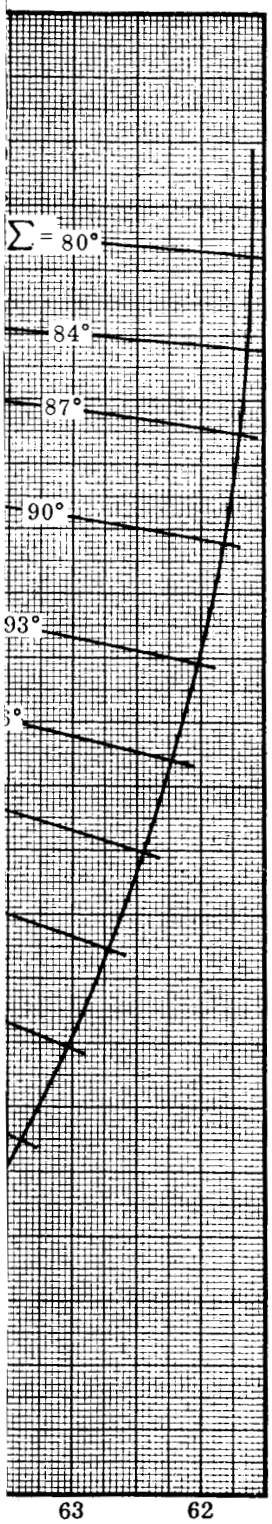

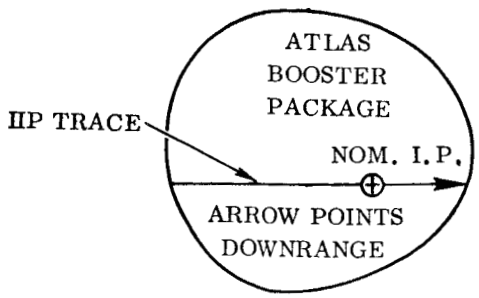

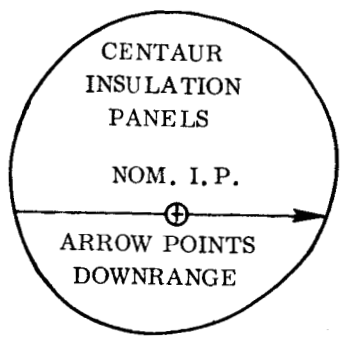

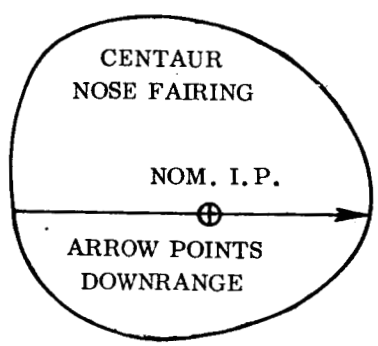

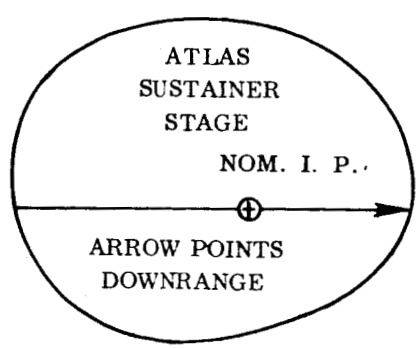

SECTION 3

DESTRUCT DATA

3.1 VEHICLE FRAGMENTATION. The number of vehicle fragments resulting from destruct action have been estimated from studies of actual Atlas destruction (Reference 9) and considerations of the structure of the vehicle. A breakdown of the number of resulting fragments is presented in Table 3-1.

Table 3-1. Estimated Number of Fragments Resulting from Propellant Explosion

TYPE	WEIGHT RANGE (lb)			
	0 - 5	5 - 25	25 - 200	> 200
No. of Booster Fragments	2300	288	127	12
No. of Sustainer Fragments	2260	280	114	9
No. of Centaur Fragments	2300	110	55	12

3.2 DRAG DATA FOR MAJOR FRAGMENTS. As requested in Reference 2, drag data for 15 major fragments are presented in Table 3-2. Choice of these fragments was based on the same criteria as for the fragmentation data presented above. The drag data were obtained by selecting proper coefficient data from References 6 and 7 for cones, cylinders, and plates as approximations to actual fragment configurations.

The expected no-wind maximum and minimum distance pieces noted in Table 3-2 were selected only on the basis of drag coefficient data. (Minimum distance - maximum drag and maximum distance - minimum drag.) No considerations were given to the initial velocity increment imparted to these fragments by an explosion. The limited information available from the AC-5 post failure investigation tends to confirm these assumptions.

3.3 EFFECT ON REMAINING STAGE. Destruct or inadvertent explosion of the propellants of either the Atlas or Centaur stages is expected to cause detonation of the propellants of the remaining stage. Flights F-1 and AC-5 are considered to be sufficient proof of this statement. An explosion on board the F-1 Centaur caused detonation of the Atlas propellants, and during the AC-5 flight, explosion of the Atlas propellants was responsible for detonation of the Centaur propellants. Therefore, it is not considered possible for Centaur to continue in powered flight following an explosion onboard Atlas.

3.4 VELOCITY INCREMENT DUE TO RELEASE OF TANK PRESSURES. Velocities due to release of tank pressure were obtained by the method of Reference 10 which is outlined in Appendix B. Since the delta velocity is a function of the area of the fragment, the maximum estimated areas were used for the calculations, thus producing the greatest possible velocity increment. The results are included in Table 3-2.

3.5 VELOCITY INCREMENT DUE TO PROPELLANT DETONATION. Velocities resulting from propellant detonation were obtained by a method which uses the blast wave equations of Reference 11. These equations, along with a discussion of their present applicability, are presented in Appendix C. Since the energy yield of the propellant detonation is a function of flight time, delta velocities were computed for the fragments over a time interval from lift-off until their respective jettison times. The computations were accomplished on a CDC 160-A digital computer.

Since the velocity imparted to the fragment depends on the distance from the origin of the explosion, detonation of the Atlas and Centaur propellants were considered separately. In both cases detonation of the propellants was assumed to occur at the intermediate bulkheads of the respective vehicles and, in each instance, effects of detonation were considered to be free from any interference by the other stage. Velocities obtained from individual Atlas and Centaur propellant detonations were then added vectorially to produce the results in Figure 3-1 and the maximum values in Table 3-2. The C_DA/W used in the computations corresponded to the maximum supersonic value of Table 3-2.

3.6 DRAG COEFFICIENTS FOR VARIOUS STAGE COMBINATIONS. In the event that flight is terminated at some time prior to orbital injection, drag coefficient data for various stage combinations have been compiled. These data are presented in Figures 3-2 through 3-6.

Table 3-2. Destruct Data for Major Fragments

ITEM	DESCRIPTION	NO. EACH	WEIGHT[1] (LB)	LOCATION[2] STATION (IN.)	LOCATION[2] RADIUS (IN.)	C_DA/W (FT^2/LB) SUBSONIC MINIMUM	C_DA/W (FT^2/LB) SUBSONIC AVERAGE	C_DA/W (FT^2/LB) SUBSONIC MAXIMUM	C_DA/W (FT^2/LB) SUPERSONIC MINIMUM	C_DA/W (FT^2/LB) SUPERSONIC AVERAGE	C_DA/W (FT^2/LB) SUPERSONIC MAXIMUM	ΔV[3] (FT/SEC)	ΔV[4] (FT/SEC)
1	Interstage Adapter	1	1636	490	60	0.0756	0.1018	0.1278	0.0880	0.1168	0.1457	159.	273.
2**	Atlas Booster Turbo-pump Assembly	1	950	1207	20	0.0067	0.0074	0.0108	0.0080	0.0089	0.0130	37.	32.
3*	Surveyor Fairing ($\frac{1}{2}$ cone + $\frac{1}{2}$ barrel)	1	592	121	39	0.0209	0.1429	0.3044	0.0315	0.2098	0.4402	171.	3192.
4	Payload Adapter	1	113	114	0	0.1108	0.2192	0.3264	0.1394	0.3514	0.5634	186.	4479.
5	Surveyor	1	2194	106	0	0.0004	0.0122	0.0237	0.0007	0.0167	0.0328	34.	269.
6	Atlas Sustainer Engine and Turbopump	1	1088	1230	0	0.0030	0.0039	0.0048	0.0056	0.0060	0.0084	43.	20.
7	Atlas Booster Engine Assembly	1	658	1240	60	0.0165	0.0206	0.0246	0.0344	0.0388	0.0431	97.	98.
8	Atlas Booster Engine Combustion Chamber	1	678	1240	60	0.0046	0.0056	0.0065	0.0102	0.0109	0.0115	50.	27.
9*	Centaur Nose Fairing ($\frac{1}{2}$ cone)	1	567	68	22	0.0208	0.1421	0.3026	0.0313	0.2086	0.4398	171.	4286.
10*	Centaur Nose Fairing ($\frac{1}{2}$ barrel)	1	425	185	38	0.0198	0.1343	0.2871	0.0296	0.1978	0.4140	170.	2356.
11	Centaur Engine Assembly	1	346	470	25	0.0202	0.0255	0.0309	0.0423	0.0482	0.0540	102.	206.
12	Centaur Engine Combustion Chamber	1	284	470	25	0.0058	0.0072	0.0085	0.0121	0.0134	0.0147	46.	57.
13*	Insulation Panels	4	249	321	55	0.0090	0.2864	0.5465	0.0141	0.3858	0.7602	297.	3262.
14	Atlas Exhaust Duct and Heat Exchanger	1	195	1250	15	0.0072	0.0186	0.0365	0.0149	0.0335	0.0637	119.	142.
15	Centaur Battery	1	67	180	40	0.0131	0.0205	0.0278	0.0207	0.0322	0.0440	72.	274.

(1) Per item
(2) Radius is distance from vehicle longitudinal axis
(3) ΔV due to internal tank pressure
(4) Maximum ΔV due to propellant detonation
*Expected no-wind minimum distance piece
**Expected no-wind maximum distance piece

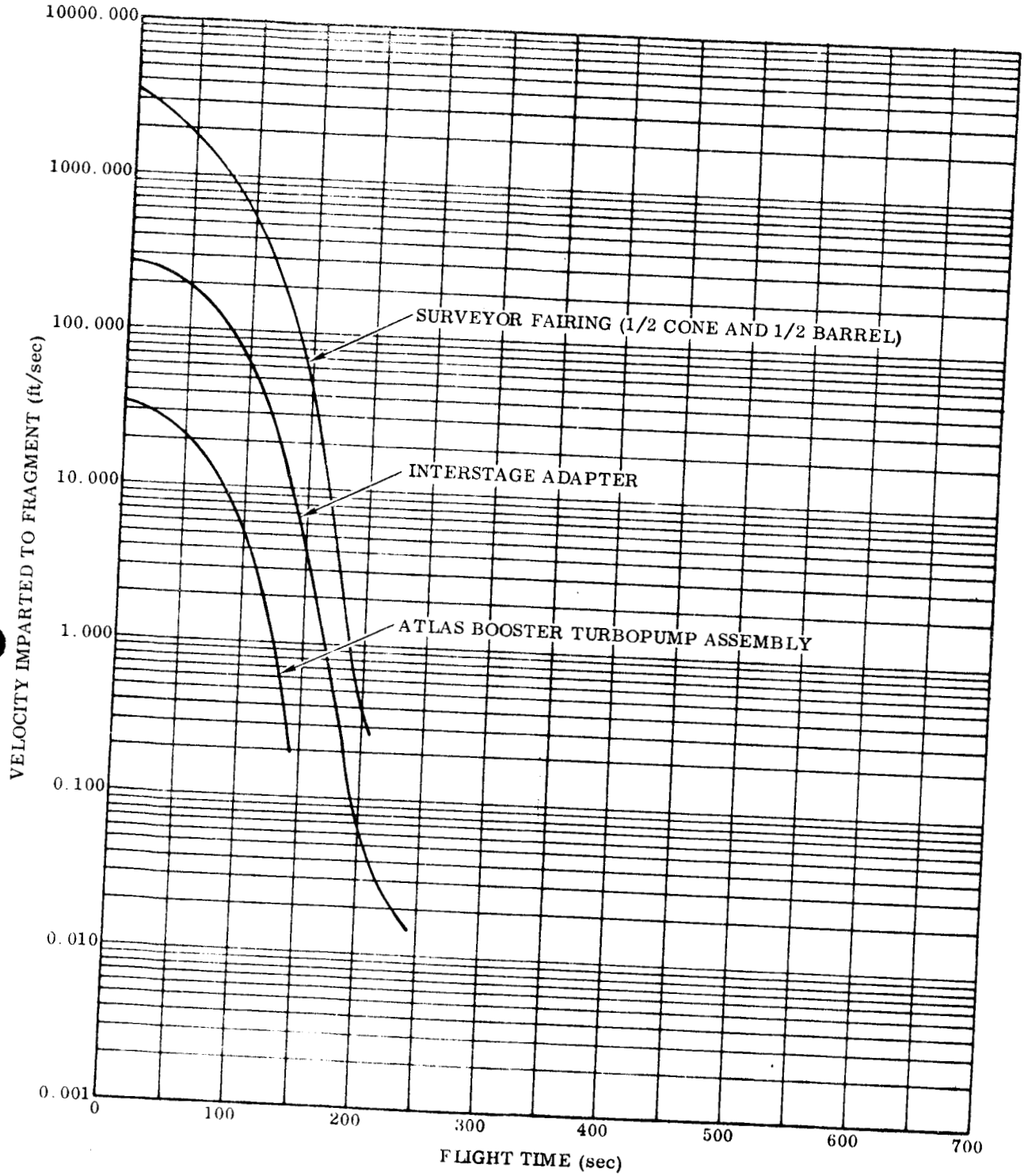

Figure 3-1. Velocity Imparted to Major Fragments by Detonation of Propellants (Sheet 1 of 5)

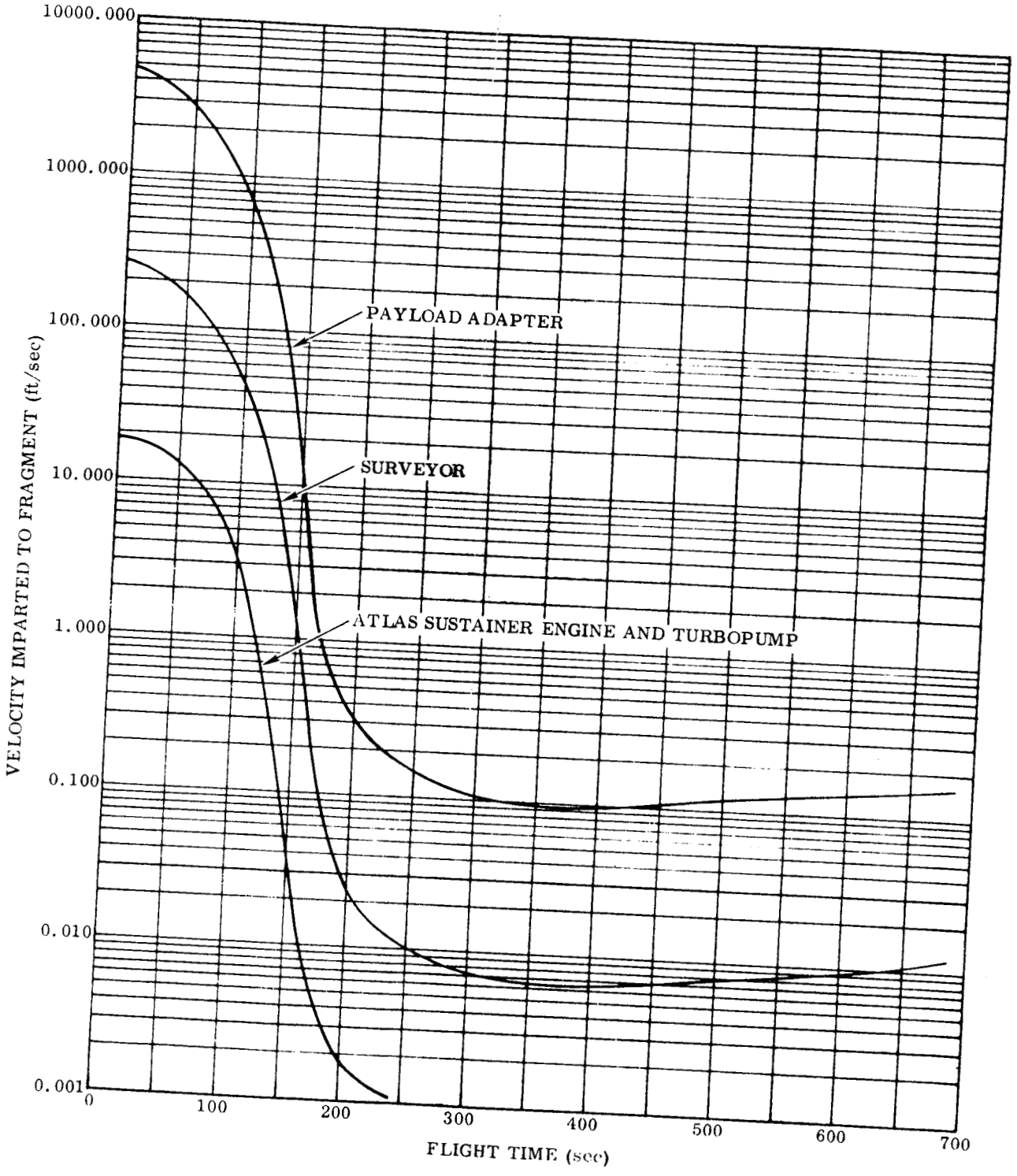

Figure 3-1. Velocity Imparted to Major Fragments by Detonation of Propellants (Sheet 2 of 5)

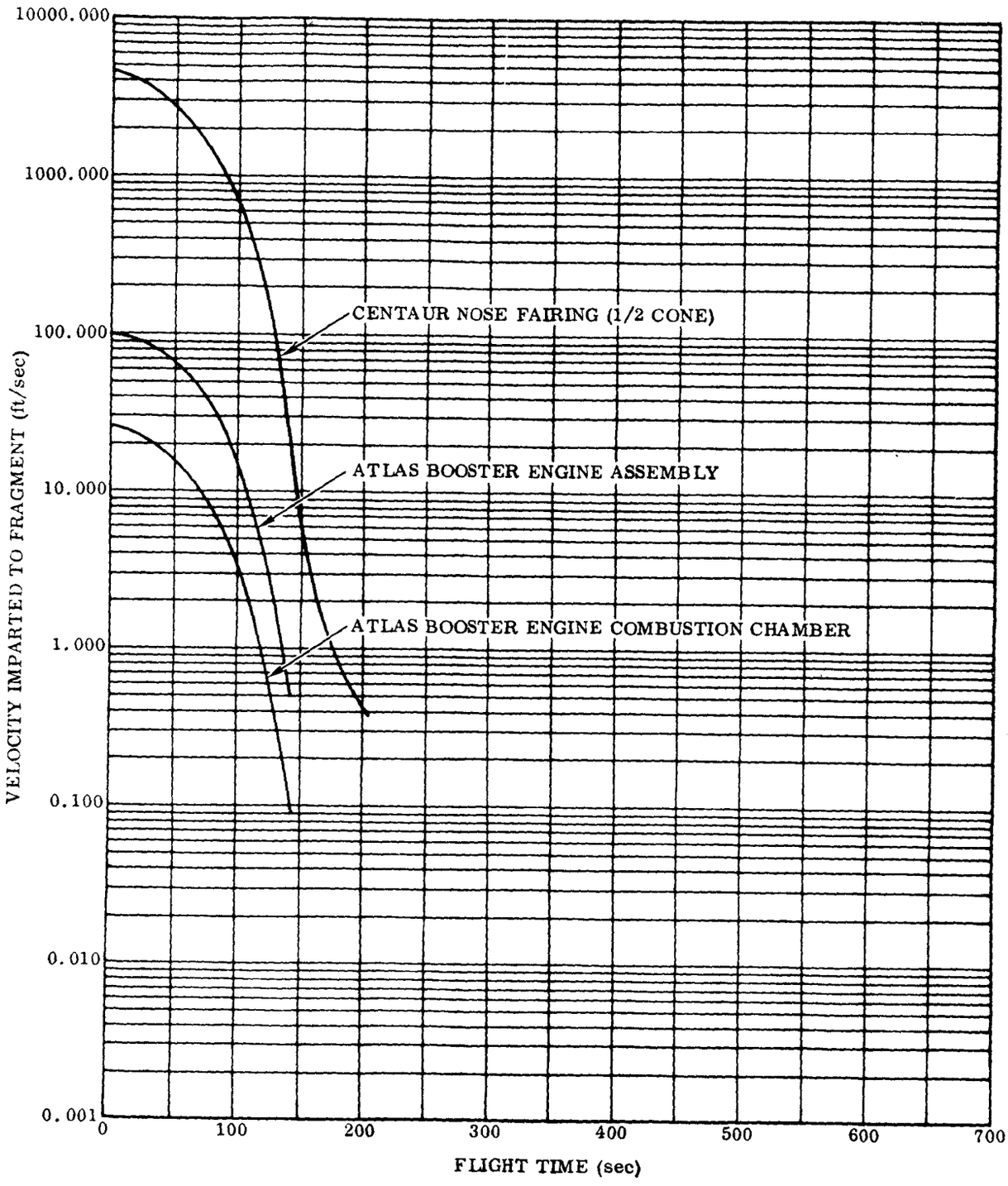

Figure 3-1. Velocity Imparted to Major Fragments by Detonation of Propellants (Sheet 3 of 5)

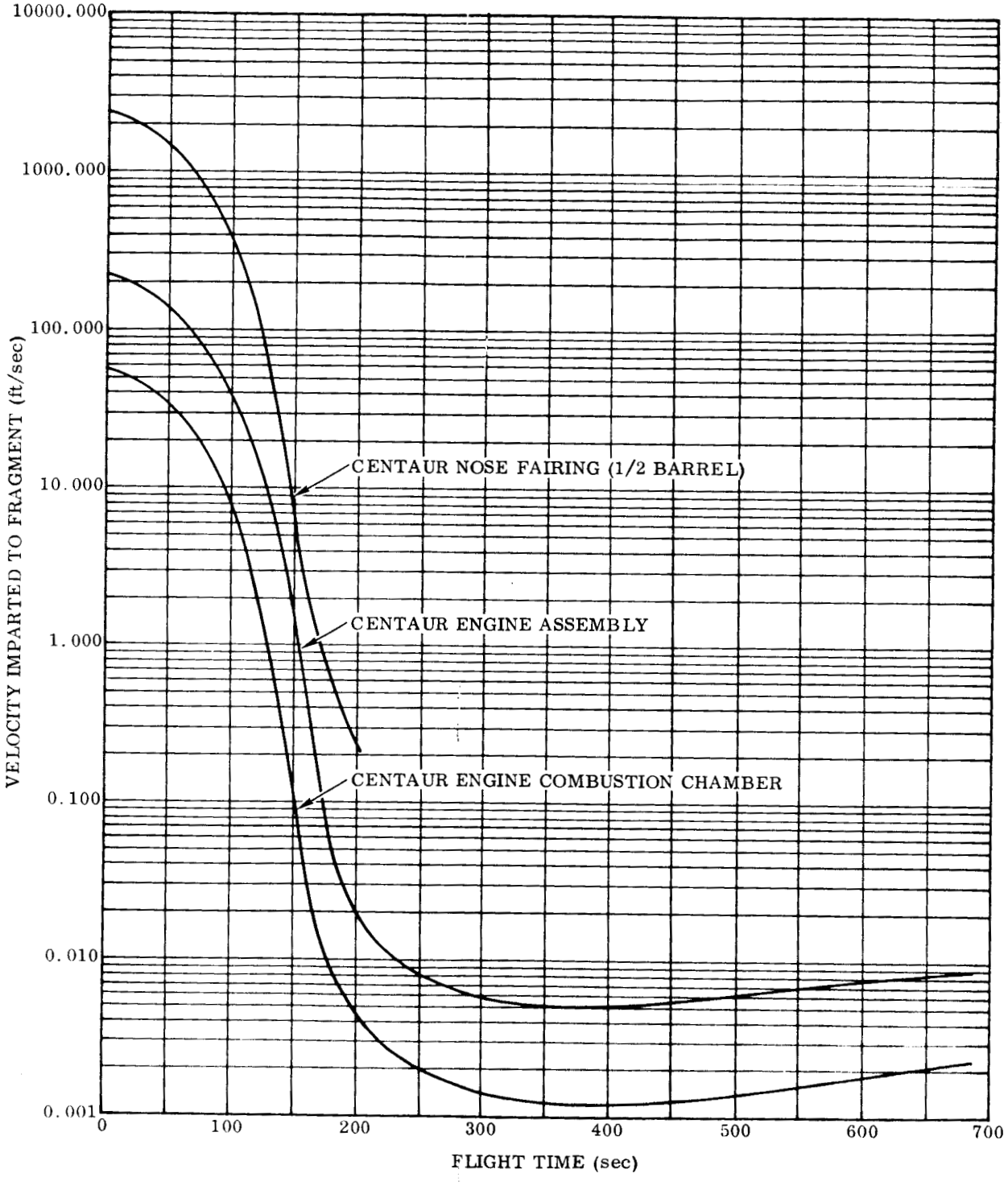

Figure 3-1. Velocity Imparted to Major Fragments by Detonation of Propellants (Sheet 4 of 5)

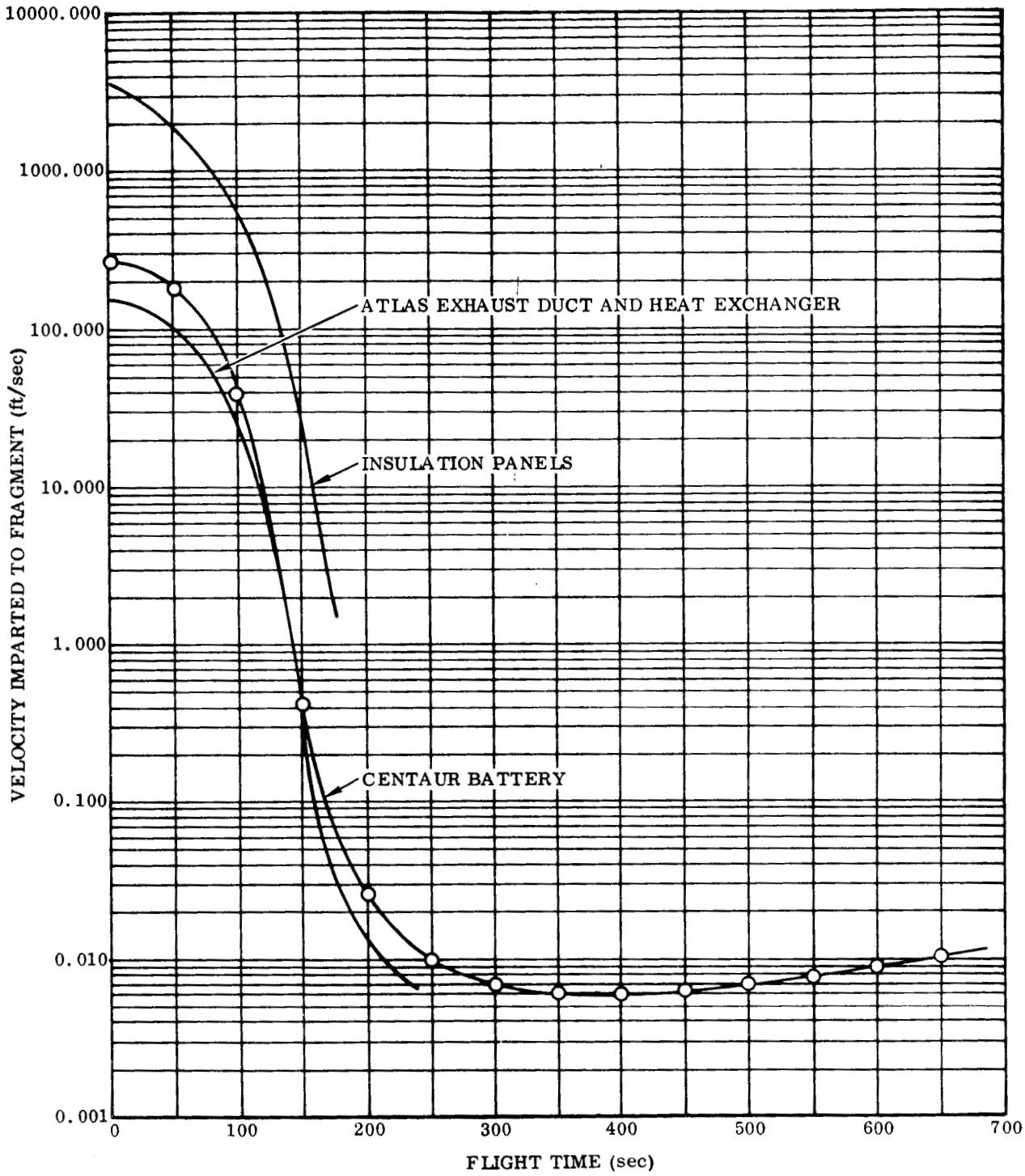

Figure 3-1. Velocity Imparted to Major Fragments by Detonation of Propellants (Sheet 5 of 5)

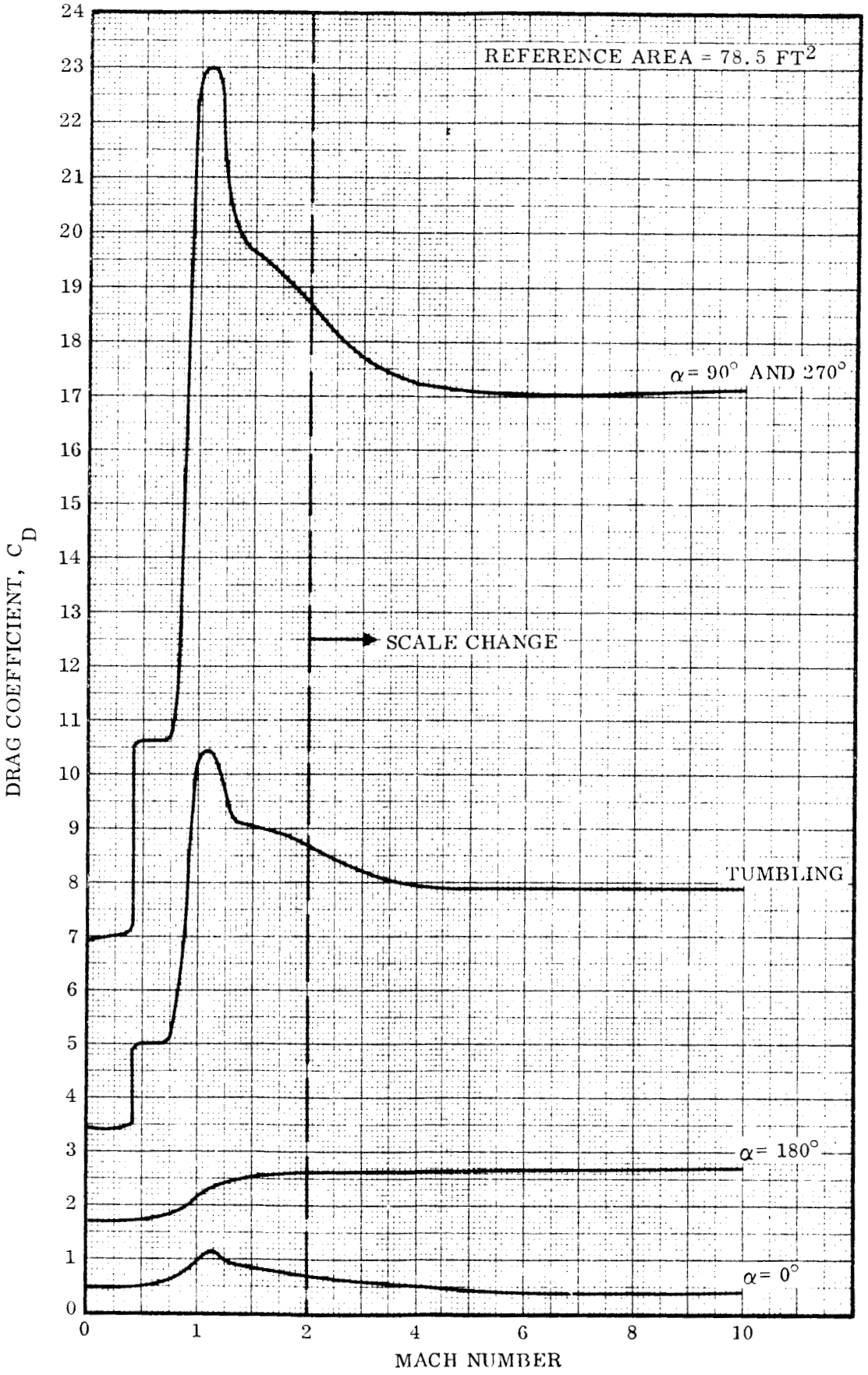

Figure 3-2. Drag Coefficients for Atlas/Centaur (Power Off)

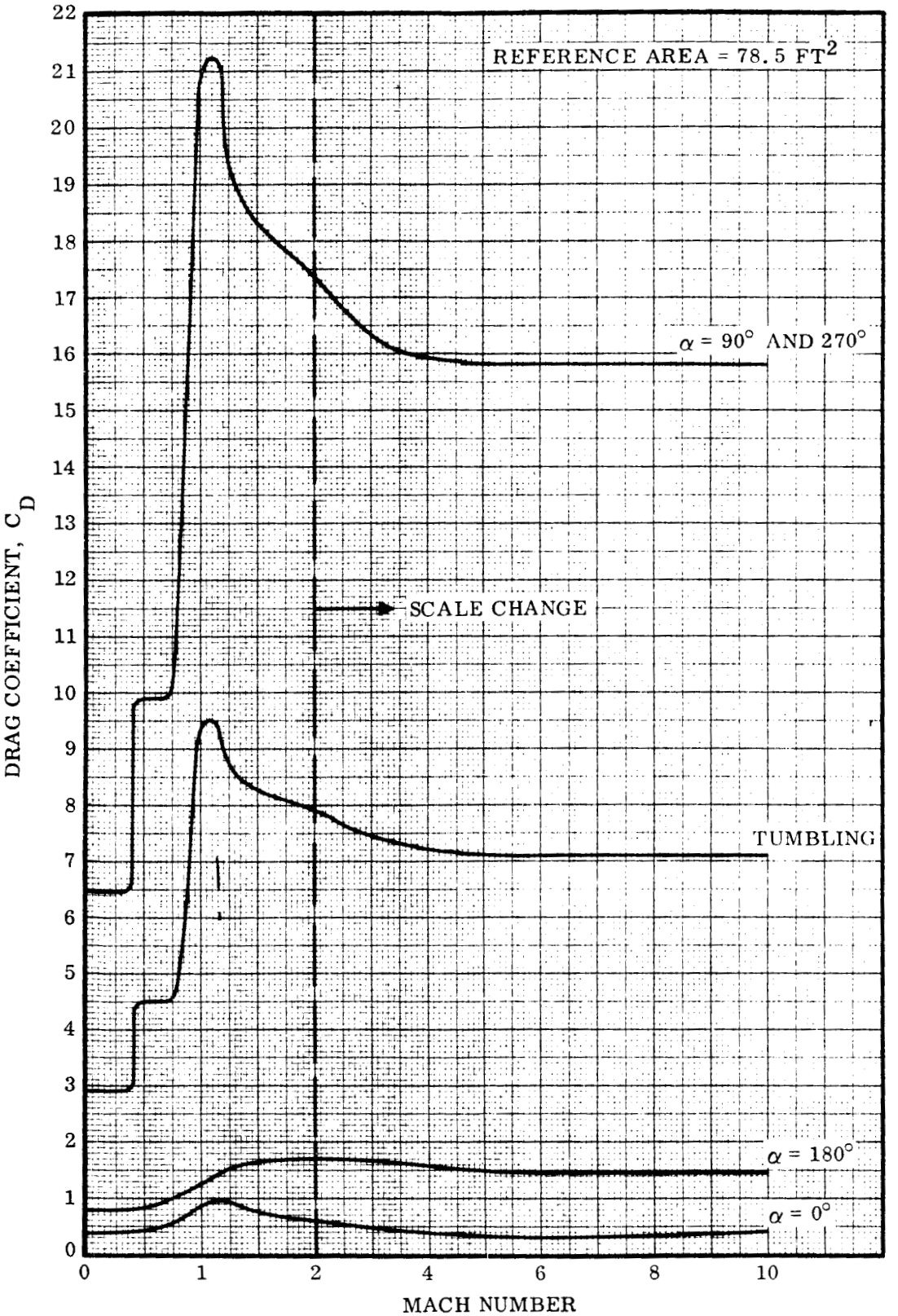

Figure 3-3. Drag Coefficients for Atlas Sustainer with Centaur (Nose Fairing and Insulation Panels Included - Power Off)

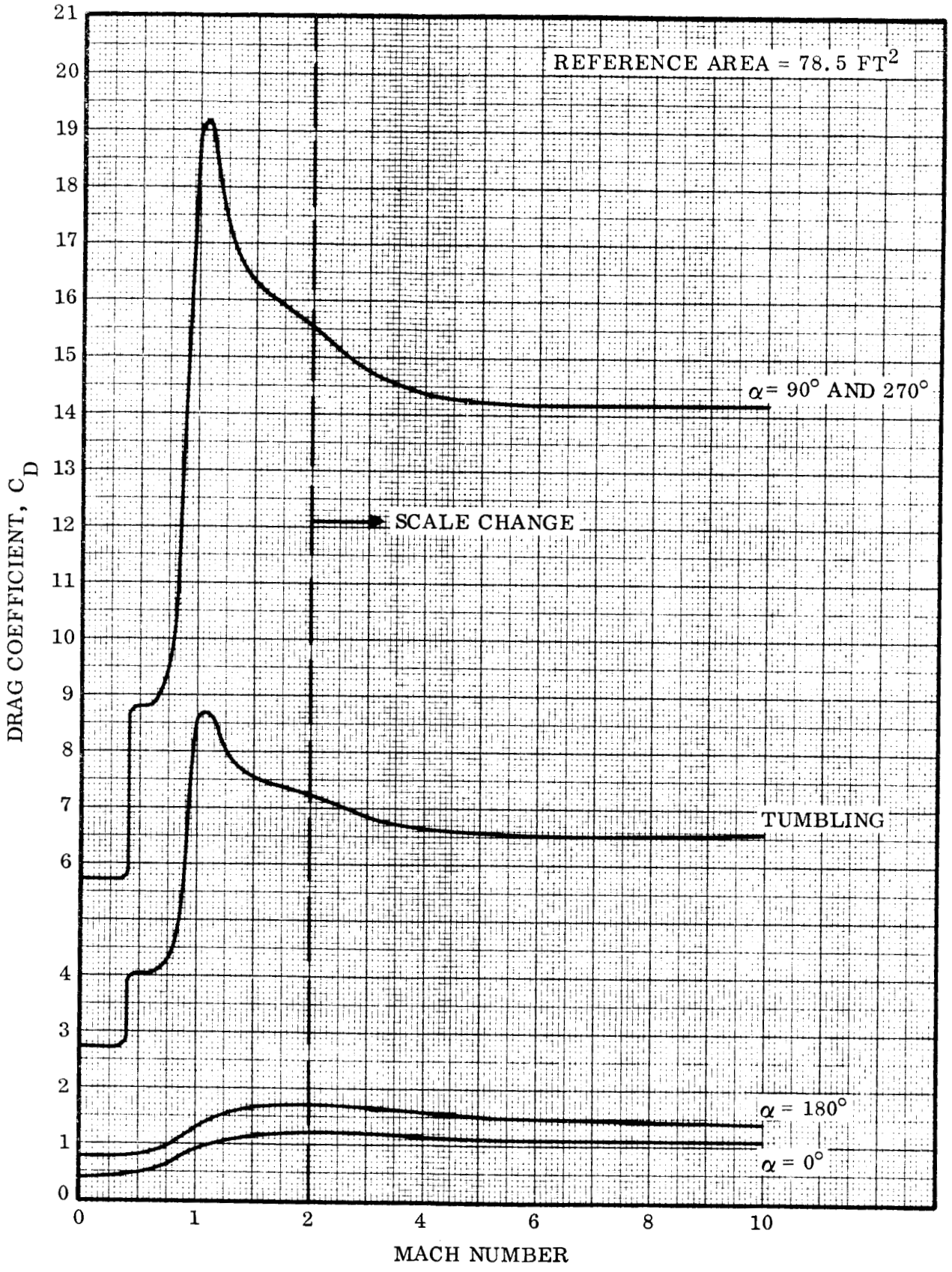

Figure 3-4. Drag Coefficients for Atlas Sustainer with Centaur (Nose Fairing and Insulation Panels Jettisoned - Power Off)

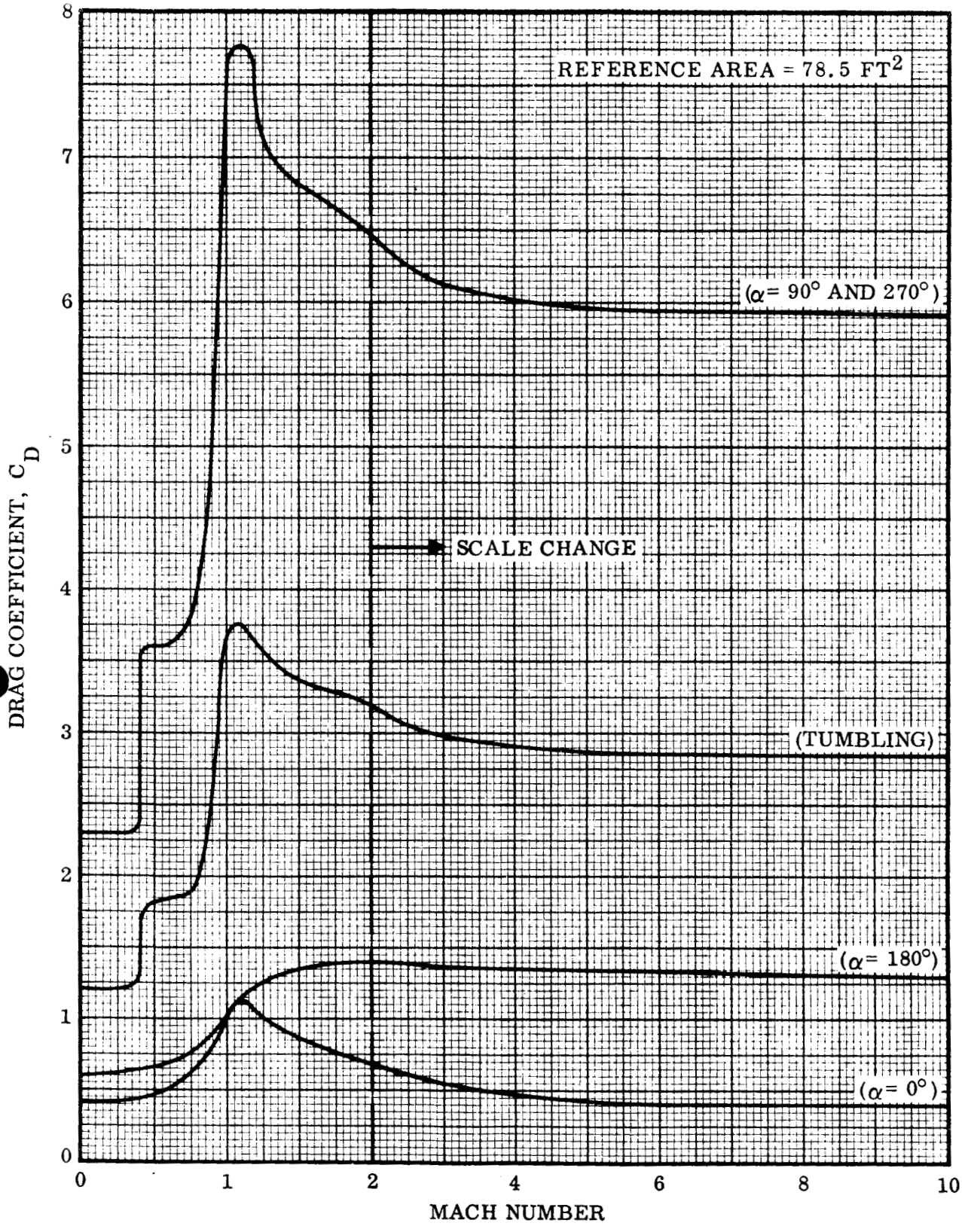

Figure 3-5. Drag Coefficients for Centaur (Nose Fairing and Insulation Panels Included - Power Off)

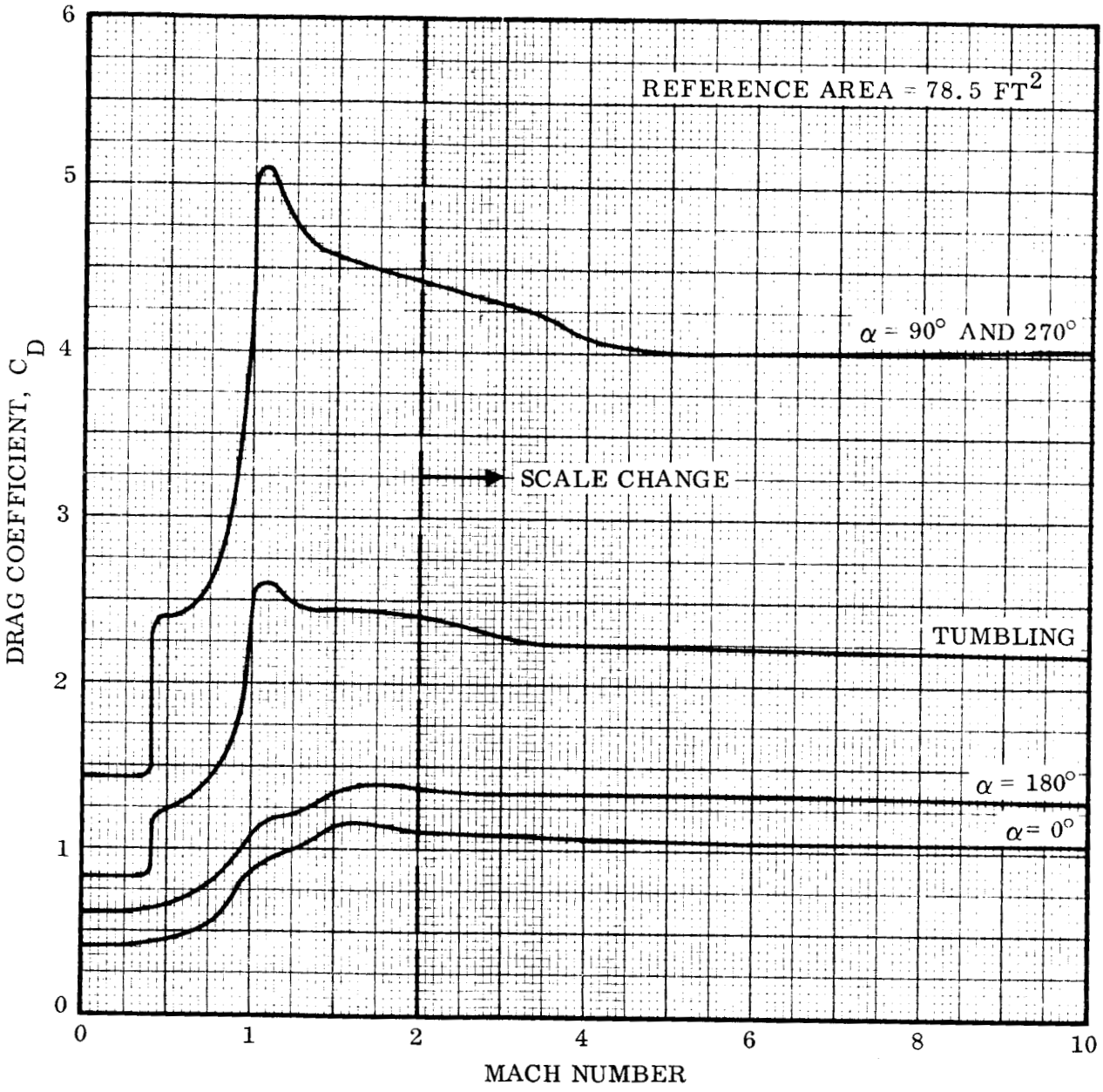

Figure 3-6. Drag Coefficients for Centaur (Nose Fairing and Insulation Panels Jettisoned - Power Off)

SECTION 4

REFERENCES

1. Letter from Headquarters Air Force Missile Test Center MTRS to distribution, Trajectory and Aerodynamic Data Requirements for Ranger, Centaur, Advent, Saint, and Similar Vehicles, 6 December 1961 (Unclassified).

2. Griffith, G., Trajectory Data Book AC-6, General Dynamics/Convair Report No. GD|C-BTD65-002, 19 April 1965 (Unclassified).

3. Hilton, H. B., The Combo Flight Program, General Dynamics/Astronautics Report GDA63-0967, 15 November 1963 (Unclassified).

4. Pavlick, T. J. and Hurlbut, B., Atlas/Centaur Range Safety and Range Planning Trajectory Data, AC-10, May-June 1966 Launch Opportunity, General Dynamics/Convair Report No. GD/C-BTD66-033, 4 April 1966.

5. Jaka, J. G., Powered Flight Simulation With Six Degrees of Freedom, General Dynamics/Convair Report No. GD/C-DBB65-016, 5 April 1966.

6. Hoerner, S. F., Fluid Dynamic Drag, published by the author, Midland Park, New Jersey, 1958 (Unclassified).

7. Welsh, C. J., The Drag of Finite - Length Cylinder Determined from Flight Test at High Reynolds Numbers for a Mach Number Range from .5 to 1.3, NACA TN 2951, June 1953 (Unclassified).

8. Smith, J. W., and Vaughn, W. W., Monthly and Annual Wind Distribution as a Function of Altitude for Patrick Air Force Base, Cape Canaveral, Florida, NASA TN D-610, July 1961 (Unclassified).

9. General Dynamics/Astronautics, Missile 1F Investigation Report, General Dynamics/Astronautics Report AC-62-0031, 17 July 1962 (Confidental).

10. Sotak, A. E. and Bizjak, F., Investigation of the Use of the Missile Fragment, Generated by the Command Destruct System, For Radar Decoys, General Dynamics/Astronautics Report ZJ-7-057, 8 May 1958 (Secret).

11. Taylor, G., The Formation of a Blast Wave by a Very Intense Explosion, Proceedings of the Royal Society, Vol. 201, 22 March 1950 (Unclassified).

12. Mysliwetz, F., Body Lift and Newtonian Theory, IAS Paper Number 62-113, June 19-22, 1962 (Unclassified).

13. Uythoven, A. and Brooks, R., Range Safety Data for the Fragmentation of an Atlas Sustainer Tank, General Dynamics/Astronautics Report ADJ-0003, 23 August 1962 (Secret).

14. Smith, O. E., A Reference Atmosphere for Patrick AFB, Florida (Annual), NASA TN D-595, March 1961.

15. Minzer, R. A., Champion, K. S. W., and Pond, H. L., The ARDC Model Atmosphere, 1959, ASTIA AD229482, (AFCRC-TR-59-267), August 1959.

APPENDIX A

AVERAGE DRAG COEFFICIENT FOR TUMBLING CYLINDER

Assume the cylinder shown in Figure A-1 is rotating about its center of gravity with constant angular velocity.

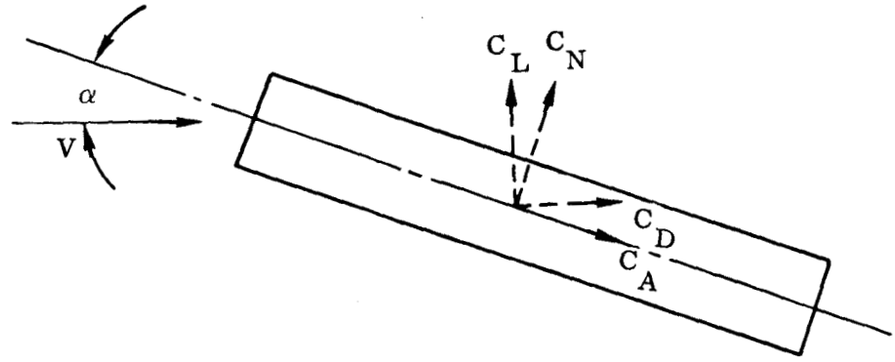

Figure A-1. Definition of Aerodynamics Terms.

Consider the rotation from $\alpha = °$ to $\alpha = 90^{\circ}$. It can be shown (Reference 12) that for either low Mach Numbers using crossflow (sweepback) theory or high Mach Numbers using Newtonian flow theory the expression for the normal force coefficient (C_N) can be written as:

$$C_N = C_{D_{90}} \sin^2 \alpha \qquad \text{A-1}$$

where $C_{D_{90}}$ is the cylinder crossflow ($\alpha = 90^{\circ}$) drag coefficient. Assume a similar variation for C_A, the axial force coefficient

$$C_A = C_{D_O} \cos^2 \alpha \qquad \text{A-2}$$

where C_{D_O} is the cylinder drag coefficient at $\alpha = 0^{\circ}$.

Using a common reference area for both C_N and C_A the following expression for C_D at any α can be written:

$$C_D = C_{D_O} \cos^3\alpha + C_{D_{90}} \sin^3\alpha \qquad \text{A-3}$$

Defining an average C_D as

$$\bar{C}_D = \frac{2}{\pi} \int_o^{\pi/2} C_D \, d\alpha \qquad \text{A-4}$$

Using equation A-3 in A-4 and integrating, the following is obtained:

$$\bar{C}_D = \frac{4}{3\pi} (C_{D_O} + C_{D_{90}}) \qquad \text{A-5}$$

Applying the same procedure for one complete revolution, the following result is found:

$$\bar{C}_D = \frac{2}{3\pi} (C_{D_O} + C_{D_{90}} + C_{D_{180}} + C_{D_{270}}) \qquad \text{A-6}$$

A similar procedure when used for the lift coefficient (C_L) produces $\bar{C}_L = O$.

Since, for relatively large aspect ratio cylinders, C_{D_O} is small compared to $C_{D_{90}}$, the assumed variation of C_A with α is not expected to introduce serious errors in $\bar{C}_D$. For Newtonian flow, the assumed variation of C_A is as valid as that used for C_N.

APPENDIX B

VELOCITIES DUE TO INTERNAL ENERGY OF PRESSURIZED TANKS

Maximum velocities imparted to the major fragments from the internal energy of the pressurized fuel and LO_2 tanks were estimated using the method of Reference 10. From Reference 10

$$\Delta V = \sqrt{\frac{2\,g\,W_k\,A}{W}}$$

where

$$W_k = \eta \frac{W_{kt}}{A_1}$$

$$W_{kt} = \frac{P_1\,V_1}{\gamma - 1}$$

A = Area of fragment (ft^2)

A_1 = Tank skin area (ft^2)

g = 32.174 ft/sec^2

P_1 = Tank pressure (lb/ft^2)

ΔV = Velocity imparted to fragment (ft/sec)

V_1 = Tank volume (ft^3)

W = Fragment weight (lb)

W_k = Energy available per square foot ($ft\text{-}lb/ft^2$)

W_{kt} = Internal energy of pressurized gas (ft-lb)

γ = Ratio of specific heats for the gas.

η = Percentage of energy transferred to the fragment.

Values used in the computations are presented in Table B-1.

Table B-1. Atlas and Centaur Tank Characteristics

TANK DESIGNATION	P_1 (lb/ft^2)	V_1 (ft^3)	γ	η	A_1 (ft^2)
Atlas LO_2	4460.0	2553.0	1.67	.23	1790.0
Atlas Fuel	8620.0	1568.0	1.67	.23	
Centaur LO_2	4610.0	375.7	1.45	.23	808.0
Centaur Fuel	3860.0	1265.4	1.70	.23	

APPENDIX C

VELOCITY IMPARTED TO A FRAGMENT BY A BLAST WAVE

From elementary aerodynamics the velocity imparted to a fragment by a blast wave is

$$\Delta V = g \frac{C_D A}{W} \int_{t=0}^{t=\infty} q\,dt \qquad \text{C-1}$$

where

A = Fragment area (ft^2)

C_D = Fragment drag coefficient

E = Energy yield of blast (ft-lb)

g = 32.174 ft/sec^2

q = Dynamic pressure (lb/ft^2)

r = Distance from blast source to fragment (ft)

R = Distance from blast source to blast wave (ft)

t = Time (sec)

t_o = Time for $\eta = 1$ (sec)

t_∞ = Time for $\eta = O$ (sec)

u = Velocity of gas (ft/sec)

ΔV = Velocity imparted to fragment (ft/sec)

W = Fragment weight (lb)

γ = Ratio of specific heats of gas

η = r / R

ρ = Density of gas ($slugs/ft^3$)

ρ_o = Atmospheric density ($slugs/ft^3$)

Equation C-1 assumes a constant $C_D A/W$ for the fragment.

The problem is one of integrating dynamic pressure over the time interval when blast wave effects are significant. A closed solution to this equation was obtained by use of the constant energy point source blast wave model of Reference 11.

From Reference 11,

$$\rho = \psi \rho_o$$

$$u = R^{-3/2} \; E^{1/2} \; B^{-1/2} \; \rho_o^{-1/2} \; \phi$$

or $$dt = E^{-1/2} \; \rho_o^{1/2} \; B^{1/2} \; R^{3/2} \; dR.$$

so that qdt becomes

$$qdt = 1/2 \rho u^2 dt = 1/2 \, \rho_o^{1/2} \; E^{1/2} \; B^{-1/2} \; \psi \; \phi^2 \; R^{-3/2} \; dR \qquad \text{C-2}$$

$$= -1/2 \, \rho_o^{1/2} \left(\frac{E}{r}\right)^{1/2} B^{-1/2} \; \psi \; \phi^2 \; \eta^{-1/2} d\eta$$

where $$\phi = \frac{\eta}{\gamma} + \left[\frac{\gamma - 1}{\gamma(\gamma+1)}\right] \eta^N$$

and $$\psi = \frac{\left(\frac{\gamma+1}{\gamma-1}\right) \eta^{\frac{3}{\gamma-1}}}{\left[\frac{\gamma + 1 - \eta^{(N-1)}}{\gamma}\right]^{\frac{2(\gamma+5)}{7-\gamma}}}$$

and $$N = \frac{7\gamma}{(\gamma^2 - 1)}$$

and $$B = 2\pi \int_o^1 4 \; \phi^2 \; \eta^2 \, d\eta + \frac{4\pi}{\gamma(\gamma-1)} \int_o^1 f \, \eta^2 d\eta$$

and $$f = \frac{\frac{2\gamma}{\gamma - 1}}{\left[\frac{\gamma+1}{\gamma} - \frac{\eta^{N-1}}{\gamma}\right]^{\frac{7\gamma^2 + 7\gamma - 3}{7 - \gamma}}}$$

To obtain fragment velocities, equation C-2 is integrated over the time interval corresponding to $\eta = 0$ to $\eta = 1$. For each time step the atmosphere relative velocity from the preceding time step is subtracted from the velocity of the shock wave. This step is included to account for atmospheric (radially inward) drag effects.

In order to account for both Atlas and Centaur propellant detonation, the two cases are computed individually and the resulting velocities added vectorially. The geometry involved in the calculations is shown in Figure C-1. For both the Atlas and Centaur vehicles the detonation is assumed to be confined to a point source originating at the intermediate bulkheads of the respective stages.

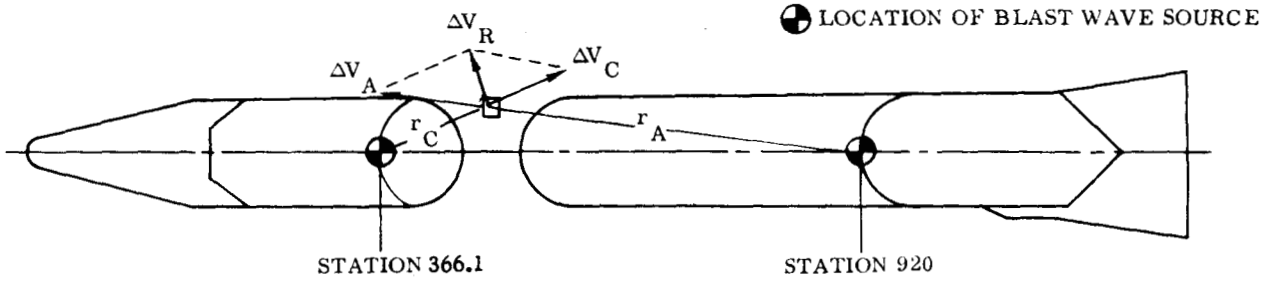

Figure C-1. Vehicle Geometry Used for Propellant Detonation Investigation